$$H_2CrO_4 + H_2O_2 = CrO_2(O_2) + 2H_2O \quad \text{rate determining} \quad (33)$$

$$CrO_2(O_2) + H_2O_2 = CrO(O_2)_2 + H_2O \quad \text{fast} \quad (34)$$

thought to involve a rate-determining substitution of the coordinated water on H_2CrO_4.[30] It is surprising to us that incorporation and loss of the second peroxide (eq 34) are such rapid processes. It may be that an increase in the coordination number of chromium(VI) accompanies formation of $CrO_2(O_2)$.

Our kinetic results strongly suggest that entry of the *second* peroxide ligand is rate-determining in the formation of oxodiperoxomolybdenum(VI). It is clear that the mechanism is more complicated than for the chromium(VI) system, where reactions 33 and 34 are independent of $[H^+]$.[30] The reaction scheme shown in eq 35-39 is consistent with the kinetic data.

$$MoO_3 + H_2O_2 = MoO_2(O_2) + H_2O \quad \text{rapid, } K_{1:1} \quad (35)$$

$$MoO_2(O_2) + H_2O_2 = MoO(O_2)_2 + H_2O \quad k_1, k_{-1} \quad (36)$$

$$MoO_2(O_2) + H_2O_2 + H^+ = MoO(O_2)_2 + H_3O^+ \; k_2, k_{-2} \quad (37)$$

$$MoO(O_2)_2 + H_2O = MoO(OH)(O_2)_2^- + H^+ \quad \text{rapid, } K_a \quad (38)$$

$$d[2:1]/dt = k_f[Mo(VI)][H_2O_2]^2 - k_r[2:1] \quad (39)$$

$$k_f = (k_1K_{1:1}/[H^+] + k_2K_{1:1})/\{([H^+] + K_a)/(1 + K_1[H^+])\}$$

$$k_r = k_{-1} + k_{-2}[H^+]$$

At 25 °C, $k_1K_{1:1} = (7.4 \pm 0.6) \times 10^6$ M^{-2} s^{-1}, $k_2K_{1:1} = (1.6 \pm 0.3) \times 10^7$ M^{-3} s^{-1}, $k_{-1} = 0.15 \pm 0.01$ s^{-1}, and $k_{-2} = (0.31 \pm 0.02$ M^{-1} $s^{-1})[H^+]$. The dioxoperoxomolybdenum(VI) species is postulated as an intermediate in low concentration. The hydrogen ion assisted pathway for the formation and dissociation of $MoO(O_2)_2$ shown in eq 37 has precedent in the $VO(O_2)^+$ and $Ti(O_2)^{2+}$ systems.[24,25] The value of the formation constant $K_{MoO(O_2)2}$ derived from the kinetic results is $7._1 \times 10^6$ M^{-1} at 25 °C, in reasonable agreement with that determined in the equlibrium study ($9._4 \times 10^6$ M^{-1}).

We detected a direct reaction between oxodiperoxomolybdenum(VI) and sulfur(IV), although it was not our original intent to do so. Very specific pathways appear to be operative in the important peroxide-sulfur(IV) systems—reaction of H_2O_2 and HSO_3^- ($k = 2.4 \times 10^6$ M^{-1} s^{-1} at 15 °C)[26] and $MoO(OH)(O_2)_2^-$ and HSO_3^- (k ca. 3×10^3 M^{-1} s^{-1} at 25 °C).

The group VIB (6^{40}) elements readily form an isostructural set of oxo diperoxo complexes under comparable experimental conditions. The formation constants appear to be very similar, although the data for the tungsten(VI) system are very limited. The interpretation of our results was greatly assisted by the extensive studies of molybdenum(VI) in acidic solution; similar studies with tungsten(VI) have not been reported. It is known that molybdenum(VI) and tungsten(VI) effectively catalyze at least some reactions of hydrogen peroxide in acidic solution.[1,17,37-39] Corresponding data for chromium(VI) are not available and would be more difficult to obtain due to the instability of $CrO(O_2)_2$ toward internal redox decomposition. Vanadium(V) promotes peroxide oxidation of iodide ion when complexed as $VO(O_2)_2^-$ (or $VO(O_2)(OOH)$) but not as the $VO(O_2)^+$ form.[25] We have found that titanium(IV) and zirconium(IV) markedly *stabilize* coordinated peroxide in acidic solution.[14-16] In our opinion the crucial factors that determine these enormously variable reactivity patterns have not been elucidated. However, comparative kinetic studies of the peroxo complexes and hydrogen peroxide coupled with a firm knowledge of the equilibrium parameters and structures of the peroxo complexes should provide important information. At the present time we can only point out that the oxo diperoxo complexes of the d^0 transition-metal ions are much more reactive than the monoperoxo forms. It seems premature to assess the specific effect of the metal ion, but other studies indicate that available coordination sites for the substrate must be present if rate enhancements are to be observed.[31]

Acknowledgment. This research was supported by the U.S. Army Research Office. Preliminary equilibrium studies were performed by Arthur Suits.

(37) Payne, G. B.; Williams, P. H. *J. Org. Chem.* **1959**, *24*, 54.
(38) Schultz, H. S.; Freyermuth, H. B.; Buc, S. R. *J. Org. Chem.* **1963**, *28*, 1140.
(39) Ogata, Y.; Kazushige, T. *Can. J. Chem.* **1981**, *59*, 718.
(40) In this paper the periodic group notation in parentheses is in accord with recent actions by IUPAC and ACS nomenclature committees. A and B notation is eliminated because of wide confusion. Groups IA and IIA become groups 1 and 2. The d-transition elements comprise groups 3 through 12, and the p-block elements comprise groups 13 through 18. (Note that the former Roman number designation is preserved in the last digit of the numbering: e.g., III → 3 and 13.)

Contribution from the Kenan Laboratories of Chemistry, The University of North Carolina, Chapel Hill, North Carolina 27514

Electrochemical Reactivity of Manganese(II) Porphyrins. Effects of Dioxygen, Benzoic Anhydride, and Axial Ligands

S. E. Creager and Royce W. Murray*

Received October 28, 1986

Currents for electrochemical reductions of manganese(III) porphyrins in oxygenated, aprotic media correspond to passage of between one and two electrons per porphyrin, depending on the experimental time scale, the axial base present, and the particular porphyrin. The two-electron process corresponds to an "ECE" reaction sequence involving formation and subsequent reduction of an intermediate Mn(II)-dioxygen adduct. The formal potential of the second electron step is shown to be ca. -0.17 V vs. NaSCE for Mn(TPP)benzoate. Passage of the second electron is suppressed by strong axial bases and by competitive axial binding but is promoted by use of an axial anion that gives the most negative potential for passage of the first electron, Mn(TPP)benzoate being a specific example. The overall rate constant for the intermediate chemical step is estimated. In the presence of the added electrophile benzoic anhydride, and on a slower time scale, reduction by more than two electrons occurs by a process postulated to involve heterolysis of the O-O bond by the electrophile, producing an even more easily reduced, high-valent manganese-oxo porphyrin. The rate of electrophile attack is slower than that for dioxygen binding.

Molecular oxygen is a strong thermodynamic oxidant but reacts only slowly with the many available reducing agents in the environment. Much effort has gone into understanding synthetic and natural catalysts[1,2] that promote the reaction of dioxygen with oxidizable substrates. The heme group is a common component of natural oxygen activation catalysts, which has prompted studies[3,4] on the interaction of dioxygen with model iron(II)

(1) *Metal Ion Activation of Dioxygen*; Spiro, T. G., Ed.; Wiley: New York, 1983.
(2) *The Biology and Chemistry of Active Oxygen*; Bannister, J. V., Bannister, W. H., Eds.; Elsevier: New York, 1984.

0020-1669/87/1326-2612$01.50/0

Table I. Cyclic Voltammetric Results for Manganese(III) Porphyrin Complexes[a]

compd	added axial base	added anion	without O_2		with O_2		
			$E°$, V	ΔE_p, mV	i_a/i_c	i_{O_2}/i_{argon}	i_a/i_c
Mn(TPP)Cl			−0.31	80	0.93	1.59	0.85
	1-MeImd		−0.28	70	0.94	1.37	0.74
	pyridine		−0.34	115	0.90	1.54	0.63
		Et_4NCl[b]	−0.29	70	0.92	1.13	0.89
	1-MeImd	Et_4NCl[b]	−0.29	70	0.91	1.20	0.97
Mn(TPP)Br			−0.31	95	0.97	1.52	0.52
	1-MeImd		−0.29	80	0.92	1.15	0.67
	pyridine		−0.25	130	0.95	1.33	0.53
Mn(TPP)OAc			−0.34	70	0.93	1.20	0.81
	1-MeImd		−0.33	80	0.90	1.18	0.84
Mn(TPP)Bzo			−0.40	60	0.90	2.41	0.49
	1-MeImd		−0.33	80	0.95	1.96	0.53
	pyridine		−0.37	110	0.84	2.61	0.46
		Me_4NBzo[c]	−0.39	60	0.93	2.09	0.51
	1-MeImd	Me_4NBzo[c]	−0.37	90	0.92	1.96	0.51
Mn(TMP)Cl			−0.49	70	0.89	1.76	0.61
	1-MeImd		−0.43	70	0.98	1.35	0.86
Mn(TMP)Bzo			−0.51	110	0.94	1.90	0.56
	1-MeImd		−0.41	90	0.94	1.34	0.86
Mn(*p*-MeOTPP)Cl			−0.37	90	0.97	1.60	0.64
	1-MeImd		−0.35	65	0.95	1.24	0.73
M(*p*-MeOTPP)Bzo			−0.40	70	0.91	1.90	0.72
	1-MeImd		−0.36	90	0.91	1.57	0.79

[a] All voltammograms were taken in dichloromethane at 20 mV/s with [Mn(Por)] = 1 mM and [axial base] = 5 mM, except as indicated. Potentials were measured and reported vs. NaSCE. Abbreviations: TPP = tetraphenylporphine, TMP = tetramesitylporphine, *p*-MeOTPP = tetrakis(*p*-methoxyphenyl)porphine, Bzo^- = benzoate, 1-MeImd = *N*-methylimidazole. [b] [Et_4NCl] = 20 mM. [c] [Me_4NBzo] = 5 mM.

porphyrins and other metalloporphyrins including cobalt,[3] manganese,[5] chromium,[6] and ruthenium[7] derivatives.

We recently[8] described a manganese porphyrin catalyzed electrochemical activation of dioxygen toward olefin epoxidation. Among the manganese and other metalloporphyrins that have been studied[9] as olefin epoxidation catalysts and as models of cytochrome P-450 reactions, a few[9f,i-k] have relied on adding chemical reducing agents to mixtures of dioxygen, metalloporphyrin catalyst, and substrate. We found[8] that supplying the reducing equivalents electrochemically to mixtures of dioxygen, metalloporphyrin catalyst, and substrate is both conceptually straightforward and experimentally advantageous in probing the individual reaction steps of the catalytic cycle.

This paper presents a more detailed study of the reactivity of dioxygen and of an acid anhydride with electrochemically reduced manganese porphyrins. The reaction between porphyrin and dioxygen is the initial phase of the catalytic epoxidation cycle.[8] It is an "ECE" process (electron transfer–chemical step–electron transfer) leading to a doubly reduced manganese porphyrin–oxygen adduct, on the basis of results from cyclic voltammetry, rotated-disk voltammetry, and chronoamperometry. The voltammetry also shows that the second phase of the catalytic epoxidation cycle,[8] a reaction between the reduced Mn(Por)–O_2 adduct and the electrophile benzoic anhydride, occurs on a time scale slower than dioxygen adduct formation. In the absence of olefin substrate, the product of this reaction is reduced in a steady-state electrocatalytic regeneration of the original manganese porphyrin complex. A reaction scheme is proposed that takes account of the roles of manganese porphyrin, axial bases and anions, dioxygen, and anhydride.

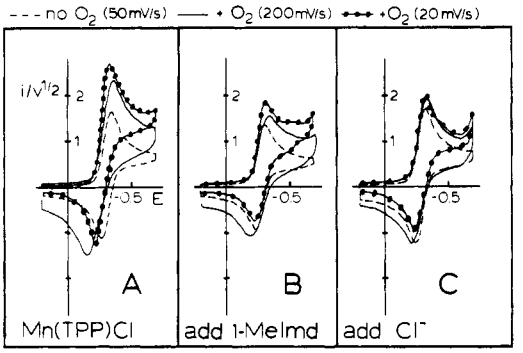

Figure 1. Cyclic voltammetry of 1.0 mM Mn(TPP)Cl in the presence (—, -●-) and absence (---) of dioxygen: (A) Mn(TPP)Cl; (B) solution in (A) plus 1-methylimidazole (10 mM); (C) solution in (A) plus Et_4NCl (20 mM). Currents are normalized by dividing by (potential sweep rate)$^{1/2}$ (μA s$^{1/2}$/mV$^{1/2}$).

Results and Discussion

Cyclic Voltammetry: Reactivity with Dioxygen. Cyclic voltammetry of CH_2Cl_2 solutions containing manganese tetraphenylporphyrin chloride, with and without dioxygen and in the presence of axial ligands, is illustrated in Figure 1.

In the absence of dioxygen (dashed line in Figure 1), peak currents for voltammograms (at comparable porphyrin concentrations) are roughly the same and increase proportionally to $v^{1/2}$,

(3) James, B. R. In *The Porphyrins*; Dolphin, D. E., Ed.; Academic: New York, 1978; Vol. 5, Chapter 6.
(4) *Iron Porphyrins*; Gray, H. B., Lever, A. B. P., Eds.; Addison-Wesley: Reading, MA, 1983.
(5) (a) Urban, M.; Kazuo, N.; Basolo, F. *Inorg. Chem.* **1982**, *21*, 3406. (b) Jones, R.; Summerville, D.; Basolo, F. *J. Am. Chem. Soc.* **1978**, *100*, 4416. (c) Hoffman, B.; Weschler, C.; Basolo, F. *J. Am. Chem. Soc.* **1976**, *98*, 5473. (d) Shirazi, A.; Goff, H. *J. Am. Chem. Soc.* **1982**, *104*, 6318. (e) Valentine, J.; Quinn, A. *Inorg. Chem.* **1976**, *15*, 1997. (f) Burstyn, J. N.; Roe, J. A.; Valentine, J. S. Presented at the 192nd National Meeting of the American Chemical Society, Anaheim, CA, Sept 1986; paper INOR 364. (g) VanAtta, R. B.; Strouse, C. E.; Hanson, L. K.; Valentine, J. S. *J. Am. Chem. Soc.* **1987**, *109*, 1425.
(6) Cheung, S.; Grimes, C.; Wong, J.; Reed, C. *J. Am. Chem. Soc.* **1976**, *98*, 5028.
(7) (a) Groves, J. T.; Quinn, R. *Inorg. Chem.* **1984**, *23*, 3844. (b) Groves, J. T.; Quinn, R. *J. Am. Chem. Soc.* **1985**, *107*, 5790.
(8) Creager, S. E.; Raybuck, S. A.; Murray, R. W. *J. Am. Chem. Soc.* **1986**, *108*, 4225.
(9) (a) Groves, J. T.; Wanatabe, Y.; McMurry, T. J. *J. Am. Chem. Soc.* **1983**, *105*, 4489. (b) Groves, J. T.; Kruper, W. J.; Haushalter, R. C. *J. Am. Chem. Soc.* **1985**, *107*, 6375. (c) Collman, J. P.; Kodadek, T.; Brauman, J. I. *J. Am. Chem. Soc.* **1986**, *108*, 2588. (d) Collman, J. P.; Brauman, J. I.; Meunier, B.; Raybuck, S. A.; Kodadek, T. *Proc. Natl. Acad. Sci. U.S.A.* **1984**, *81*, 3245. (e) Renauk, J. P.; Battiono, P.; Bartioli, J.; Mansuy, D. *J. Chem. Soc., Chem. Commun.* **1983**, 888. (f) Mansuy, D.; Fontecabe, M.; Bartioli, J. *J. Chem. Soc., Chem. Commun.* **1983**, 253. (g) Yuan, L. C.; Bruice, T. C. *J. Am. Chem. Soc.* **1986**, *108*, 1643. (h) Smegal, J. A.; Hill, C. L. *J. Am. Chem. Soc.* **1983**, *105*, 3515. (i) Tabushi, I.; Morimitsu, K. *J. Am. Chem. Soc.* **1984**, *106*, 6871. (j) Tabushi, I.; Yazaki, A. *J. Am. Chem. Soc.* **1981**, *103*, 7371. (k) Perree-Fauvet, M.; Gaudemer, A. *J. Chem. Soc., Chem. Commun.* **1981**, 874.

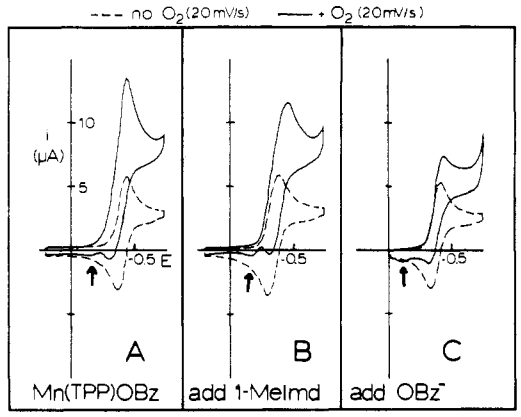

Figure 2. Cyclic voltammetry (20 mV/s) of Mn(TPP)Bzo (1.0 mM) in the presence (—) and absence (---) of oxygen: (A) Mn(TPP)Bzo; (B) solution in (A) plus 1-methylimidazole (5 mM); (C) solution in (A) plus tetramethylammonium benzoate, saturated (approximately 20 mM).

the ratio of oxidation to reduction peak currents (i_a/i_c) is near unity, and the reactions are quasi-reversible (70–115-mV ΔE_p separation between oxidation and reduction peak potentials; see Table I). These results, and a coulometric determination (vide infra), point to a diffusion-controlled, one-electron electrochemical reduction in the absence of dioxygen.[10] Similar results are obtained for other manganese metalloporphyrins (Table I); values of the formal potentials $E^{\circ\prime}$ of the voltammetric waves vary of course with the particular porphyrin and added ligand.

Addition of dioxygen to the metalloporphyrin solutions invariably results in reduction currents larger than those seen in its absence; see the i_{O_2}/i_{argon} column in Table I. The magnitude of the effect depends on the potential sweep rate. In the case of a mixture of dioxygen and Mn(TPP)Cl in Bu_4NClO_4–CH_2Cl_2 (Figure 1A) the peak reduction current is enhanced by dioxygen by a factor of 1.59 at 20 mV/s (-●-), by 1.39 at 200 mV/s (—), and by very little at 500 mV/s (not shown). (Note that currents in Figure 1 are normalized to (potential sweep rate)$^{1/2}$ to facilitate identification of diffusional vs. other sweep rate dependences.) The potential sweep rate behavior shows that some step with a kinetic rate comparable to the potential sweep time scale controls the magnitude of the enhanced reduction current; from previous literature we guess that this step involves the binding of dioxygen to reduced Mn(II) porphyrin to give a adduct that can be reduced by a second electron.

Addition of 1-methylimidazole, chloride ion, or both to Mn(TTP)Cl solutions produces a diminished current enhancement in the presence of dioxygen, as seen in Figure 1B,C. Nitrogenous bases have a generally similar effect for other manganese porphyrins (see Table I, i_{O_2}/i_{argon} column). Again, the current enhancements show reaction kinetic limitations as evidenced by the diminution of the current enhancement at higher potential sweep rates.

Cyclic voltammetry of the manganese(III) tetraphenylporphyrin benzoate complex Mn(TPP)Bzo (Figure 2) differs from that of the other Mn(TPP)X complexes in three important ways. First, the formal potential for the Mn(III/II) reduction of this complex in the absence of dioxygen (---) is the most negative of the series (Table I). Second, the reduction current in the presence of dioxygen (—) is enhanced (relative to that under argon) to the greatest extent (2.41X) with the benzoate complex. This means that the benzoate complex leads to more facile dioxygen adduct formation and reduction. Third, the voltammetric reoxidation

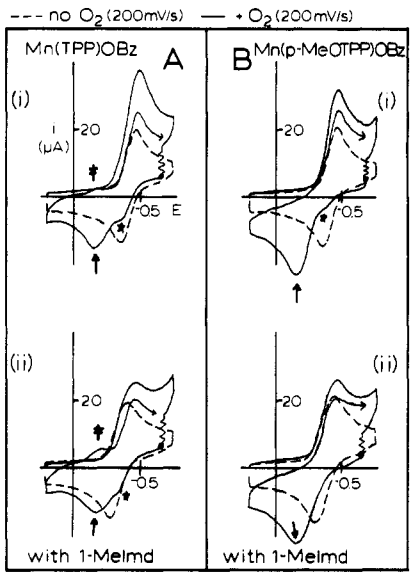

Figure 3. Modified cyclic voltammograms of Mn(Por)Bzo complexes under argon (---) and O_2 (—) (see text): (A) Mn(TPP)Bzo (i) with no axial base and (ii) plus 1-methylimidazole (5 mM); (B) Mn(*p*-MeOTPP)Bzo with (i) no axial base and (ii) plus 1-methylimidazole (5 mM). Jagged lines and ● indicate where the potential scan was temporarily (~30 s) halted.

wave in Figure 2 in the presence of dioxygen both is less prominent and is split into two steps.

These data and those for other manganese porphyrins (Table I), with added axial anions and nitrogenous bases, are strongly consistent with an ECE electrode mechanism or its close relative $DISP_1$.[10] In either case, reduction by one electron to the Mn(II) porphyrin is followed by a chemical step or steps that promote transfer of a second electron. Given the prior literature[5,9a] on reduced manganese porphyrins, it is reasonable to assume that the intermediate chemical step includes dioxygen binding to give a further reducible Mn–O_2 adduct. If the chemical step were fast on the voltammetric time scale, the reduction current would correspond to that for a net two-electron reaction, and i_{O_2}/i_{argon} would equal 2.8/1, the odd number arising from the $n^{3/2}$ dependency in the Randles–Sevcik equation.[11] The chemical step apparently has slower rates than this, however, since in all of our experiments (Table I) the i_{O_2}/i_{argon} ratio is between 1 and 2.8.

It appears in these results that variation of the formal potential $E^{\circ\prime}$ for the Mn(III/II) reduction step with the axial anion of the parent complex has consequences in values of i_{O_2}/i_{argon}. Significantly, for each of the porphyrins in Table I the benzoate complex exhibits both the most negative Mn(III/II) reduction potential and the most facile dioxygen binding and adduct reduction as measured by the enhanced reduction currents in the presence of dioxygen. In a classical ECE electrochemical reduction reaction, the formal potential $E^{\circ\prime}_1$ for the first electron transfer is more negative than that for the second ($E^{\circ\prime}_2$), so that the second electron transfer occurs spontaneously following the chemical step. *The rate of the chemical step can, however, be influenced by the size of the ($E^{\circ\prime}_1 - E^{\circ\prime}_2$) difference, particularly if somewhat unfavorable chemical equilibria are part of the chemical step.* Thus, all other things being equal,[12] a large $E^{\circ\prime}_1 - E^{\circ\prime}_2$ difference promotes faster chemical passage of the second electron.

The above points are amplified by the hybrid voltammograms in Figure 3, where the ECE nature of the electrode reaction is

(10) (a) Bard, A. J.; Faulkner, L. *Electrochemical Methods*; Wiley: New York, 1980. (b) Amatore, C.; Gabriel, M.; Saveant, J. M. *J. Electroanal. Chem. Interfacial Electrochem.* **1983**, *147*, 1. (c) In the ECE mechanism, the electrode delivers the second electron, whereas a Mn(II) porphyrin is the reductant in the $DISP_1$ mechanism. These mechanisms have such similar behavior as to be indistinguishable in the present data, and we will cast further discussion in terms of the more conventional ECE picture.

(11) Randles–Sevcik equation for peak current in linear sweep voltammetry: $i_p = (2.69 \times 10^5)n^{3/2}AD_0^{1/2}v^{1/2}C_0^*$.

(12) Note that it is actually the $E^{\circ\prime}_1 - E^{\circ\prime}_2$ difference that is important, not just how negative $E^{\circ\prime}_1$ is. We thus implicitly assume that the porphyrin axial anion is of less consequence on the value of $E^{\circ\prime}_2$ than on $E^{\circ\prime}_1$ (within a series of complexes). We also avoid comparing $E^{\circ\prime}_1$ values for different porphyrin bases (i.e., TPP vs. TMP) because the effect of the porphyrin base on the value of $E^{\circ\prime}_2$ and on dioxygen binding *kinetics* is harder to anticipate.

unambiguously established[13] by observation of a voltammetric couple (→ and ‡) with an $E^{\circ\prime}$ more positive than the original reduction process. In the presence of dioxygen (—), the negative-going potential scan is stopped at ● to permit buildup of a solution of the reduced manganese complex within the diffusion layer around the electrode. Then, a positive potential scan is started (from ●) to observe reoxidation of the reduced complex. For both the Mn(TPP)Bzo and Mn(*p*-MeOTPP)Bzo complexes, this experiment reveals *two* different oxidation steps (at * and →). In the positive-potential scan in Figure 3A for Mn(TPP)Bzo, with and without axial base, the first oxidation wave (*) appears at the potential appropriate (compare to ---, without O_2) for reoxidation of singly reduced manganese(II) porphyrin that did not react with oxygen during its residence time in the diffusion layer. Following that, there is a second (and more prominent) wave at a more positive potential (→), for which in a second negative-going potential sweep it is significant that we see a rereduction counterpart (‡).

We attribute the second, more positive wave (→, ‡) to a redox reaction (oxidation and rereduction) of the doubly reduced Mn–O_2 adduct. Since the adduct is a reversible, transient couple, we label the process as EC_rE electrochemistry,[10a] where *the chemical step is reversible.* The position of the more positive wave (ca. −0.17 V) estimates, then, the formal potential $E^{\circ\prime}{}_2$ for the reaction

$$Mn^{III}(TPP)O_2^- + e^- \rightleftarrows Mn^{III}(TPP)O_2^{2-} \qquad (1)$$

The value of this potential, which we expect[12] not to depend on the initial axial anion, explains why the second wave is not seen in the voltammograms of Figure 1. There, the first electron transfer occurs at potentials too closely coincident to $E^{\circ\prime}{}_2$ to resolve the two processes. Also, the singly reduced $Mn^{III}(TPP)O_2^-$ adduct may undergo disproportionation so that only a small amount persists to display its rereduction step (wave ‡).

In the Mn(*p*-MeOTPP)Bzo complex voltammetry (Figure 3B), the positive-potential scan shows only a minor peak (*) for unreacted Mn^{II}(Por), and most of the current appears in the wave (→) for oxidation of the doubly reduced Mn^{III}(*p*-MeOTPP)O_2^{2-} adduct. Also there is no evidence for a rereduction wave for Mn^{III}(*p*-MeOTPP)O_2^-, indicating that this species is very reactive on the cyclic voltammetric time scale. The contrast between parts A and B of Figure 3 emphasizes how sensitive the observation of a *complete* EC_rE voltammetric pattern (seen in Figure 3A) is to the particular combination of electrochemical potentials and chemical reaction kinetics and equilibria.

At this point, it is helpful to review what is known about the axial ligation of manganese porphyrins. Kadish and Kelly,[14] and more recently Bruice,[9g] have shown that, in the presence of added axial ligand L, manganese(III) tetraphenylporphyrin exists as a mixture of Mn(Por)X, Mn(Por)XL, and Mn(Por)L_2^+ and the equilibrium constant for complexation of the first axial ligand (L) is greater than that for the second. Furthermore, reduction of Mn(Por)L_2^+ proceeds with loss of one axial imidazole, while reduction of Mn(Por)XL does not, as inferred from $E^{\circ\prime}$ vs. log [L] data. We have observed that $E^{\circ\prime}$ for Mn(TPP)Cl reduction is independent of modest concentrations (<100 mM) of added chloride, so reduction under these conditions occurs without loss of chloride from the manganese(II) state.

The stoichiometric, low-temperature reaction of dioxygen with chemically reduced manganese porphyrins was studied spectroscopically by Basolo[5a-c] and others,[5d-f] and the product is formulated as a Mn(III)–superoxide adduct. Dioxygen reacts with four-coordinate manganese(II), and so the presence of axially bound pyridine was seen to inhibit the reaction competitively.

On the basis of this prior literature and our data, we propose the EC_rE mechanism in Scheme I. The initial electron transfer

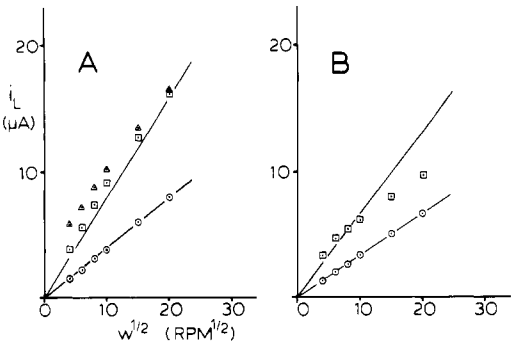

Figure 4. Levich plots of limiting currents for reduction of (A) Mn(TPP)Bzo (0.5 mM) measured at −0.55 V and (B) Mn(TPP)Bzo plus 1-methylimidazole (5 mM) at −0.40 V, in dichloromethane and 0.5 M Bu_4NClO_4: (○) under argon; (□) under dioxygen; (△) with 0.22 M benzoic anhydride and dioxygen. See ref 15.

Scheme I

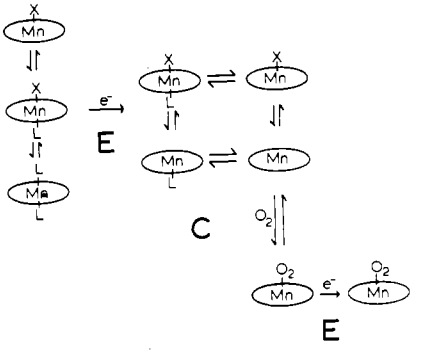

may involve any of the three different Mn(III) coordination states, depending on their proportions and interconversion rates. The reduced complex may exist in any of the four coordination states shown in the intermediate square scheme, but the concentrations of these states are not necessarily in an equilibrium distribution since we only observe the scheme within the nonequilibrium diffusion layer near the electrode surface. The binding reaction leading to the Mn^{III}(Por)O_2^- adduct occurs within the diffusion layer, whereupon this species may diffuse to the electrode surface and accept a second electron (ECE pathway) or alternatively be reduced[10b] by a Mn(II) porphyrin ($DISP_1$ pathway). The scheme emphasizes that the intermediate chemical step is *not simply that of oxygen binding* but is a *reversible composite* of (i) equilibrium constants and on–off rate constants for axial ligation to manganese(II), (ii) the equilibrium constant and on–off rates of oxygen binding, and (iii) mass transport of all of these species near the electrode surface.

Rotated-Disk Voltammetry: Reactivity with Dioxygen. Electrochemical evidence supporting Scheme I was found by manipulating the size of the diffusion layer with the electrode rotation rate in rotated-disk-electrode voltammetry. These experiments were done with the Mn(TPP)Bzo complex, which shows the greatest extent of dioxygen binding and reduction. Figure 4 shows Levich plots[10a] of limiting currents for metalloporphyrin reduction waves with (□) and without (○) dioxygen and with (panel B) and without (panel A) 1-methylimidazole axial base. For a mass-transport-controlled reaction, such a plot should be[10a] linear, with zero intercept and slope proportional to the number of electrons passed. In the absence of axial base (Figure 4A) the Levich plots are linear both with and without dioxygen, and the slope of the Levich line in the presence of dioxygen is nearly twice that in its absence.[15] Thus, within the time scale of transport through the relatively thick diffusion layers produced at these slow electrode rotation rates, formation and reduction of the $Mn^{III}(TPP)O_2^-$ adduct is fast. In contrast, the addition of 5 mM 1-methyl-

(13) A reviewer suggested that the two waves (→ and ‡) might represent the reaction of uncomplexed Mn(TPP), but these waves then should be observable in Figure 3 in the absence (---) as well as the presence (—) of dioxygen, and they are not.

(14) (a) Kelly, S. L.; Kadish, K. M. *Inorg. Chem.* **1982**, *21*, 3631. (b) Kadish, K. M.; Kelly, S. L. *Inorg. Chem.* **1979**, *18*, 2968.

(15) The kinematic viscosity of dichloromethane at 25 °C is 3×10^{-3} cm^2/s. The best line without O_2 gives $D = 5 \times 10^{-6}$ cm^2/s.

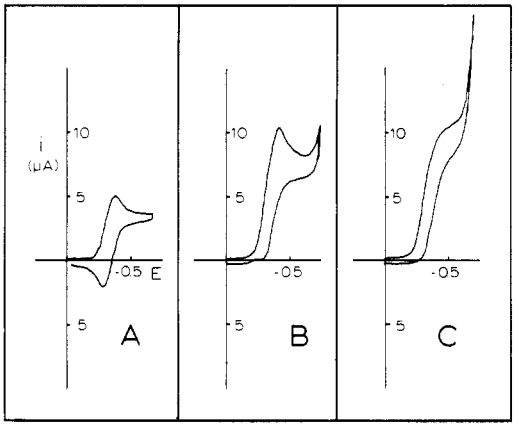

Figure 5. Cyclic voltammetry (20 mV/s) of Mn(TPP)Bzo (1.0 mM) and 1-methylimidazole (5 mM) showing the effect of anhydride: (A) under argon; (B) under oxygen; (C) under oxygen with 0.10 M benzoic anhydride present.

imidazole (Figure 4B, □) causes the limiting currents at higher rotation rates to fall below the two-electron slope. In agreement with the cyclic voltammetric data, Figure 4B confirms that axial bases diminish the overall rate of dioxygen binding and adduct reduction.

Reactivity with Acid Anhydrides. Another aspect of the reduction of dioxygen via metalloporphyrins is O–O bond heterolysis in the reduced O_2 adduct, a crucial step in most schemes for dioxygen activation. There is some debate as to what molecules act as activators in the cytochrome P-450 class of monooxygenase enzymes; protons,[16] carboxylates,[17a] and amides[17b] have all been suggested. The reaction of reduced iron porphyrin–dioxygen adducts with acid anhydrides has been shown to cleave the O–O bond.[18] Also, Groves and co-workers[19] and others[5f] have shown that benzoyl chloride reacts with a reduced manganese porphyrin–dioxygen adduct at low temperature to produce a stable acyl–peroxy manganese porphyrin complex that upon warming to room temperature decomposes by O–O bond heterolysis to produce a high-valent manganese–oxo species and carboxylate.

We exploited[8] the reaction of reduced manganese tetraphenylporphyrin–dioxygen adducts with benzoic anhydride in our catalytic-epoxidation experiments and give some further results on this reaction here. Figure 5B shows the current enhancement caused by oxygenating a solution of Mn(TPP)Bzo and 1-methylimidazole (compare to Figure 5A), and Figure 5C shows that addition of benzoic anhydride *further enhances* the cyclic voltammetric currents for dioxygen reduction via Mn(TPP)Bzo. The enhancement is not large, but the voltammetric wave shape has substantially changed, from that for a pure two-electron reduction to that of a steady-state electrocatalytic reduction.

Rotated-disk voltammetry at low rotation rates (Figure 4A, △) confirms the current enhancement by benzoic anhydride. The Levich plot for the reduction of Mn(TPP)Bzo in the presence of dioxygen and 0.22 M benzoic anhydride gives, at fast rotation rates, limiting currents (△) similar to those seen without anhydride (□, net two-electron reduction). At low rotation rates, however, the limiting currents in the presence of the anhydride are clearly *larger than those on the two-electron line* and do not extrapolate to zero at the intercept. This is diagnostic evidence for a steady-state catalytic current, which is proposed to occur via regeneration of the original, reducible Mn(III) complex. In

Scheme II

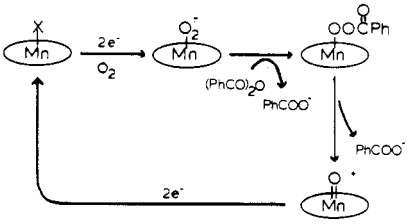

principle, the rate of such a catalytic regeneration is measurable by extrapolating observed currents to zero rotation rate,[10a] but to do so reliably in the present case required data at rotation rates lower than we could obtain.

The proposed basis of the catalytic regeneration is outlined in Scheme II. The initial reduction–dioxygen binding–reduction sequence (Scheme I) is fast on the time scale of Scheme II as demonstrated by the comparison (□, △) in Figure 4A. Whether the reaction of reduced adduct with anhydride or the subsequent decomposition to high-valent oxo–manganese porphyrin complex (and another equivalent to benzoate) is the slower step in Scheme II is unclear. The high-valent complex has interesting and potentially useful properties, including reactivity with olefins to produce epoxides.[9] The formal potential of the high-valent manganese–oxo complex is rather positive,[19] so that it is rapidly reduced to the original manganese(III) complex at the potentials employed in these experiments.

Chronoamperometry. It is desirable to at least estimate the overall rate constant for the intermediate chemical steps in Scheme I. ECE systems with characteristics amenable to kinetic quantification are in fact not numerous. We employed potential-step chronoamperometry, in which the electrode potential is stepped to a value on the limiting-current plateau and current is measured as a function of time. Information on reactivity over a wide time scale is obtained in this experiment.

Chronoamperometric results for solutions like those used in Figure 4 in rotated-disk studies are presented as Cottrell plots (current vs. $t^{-1/2}$) in Figure 6A,B. As should be the case for a diffusion-controlled reaction,[10a] a linear plot with zero intercept is obtained for reduction of Mn(TPP)Bzo in the absence of dioxygen. The addition of dioxygen doubles the slope of the Cottrell plot (Figure 6A), consistent with a two-electron reduction on this time scale. When 3 mM 1-methylimidazole is added, on the other hand (Figure 6B), the Cottrell plot attains a two-electron slope only at very long times (≥10 s) and folds over to approach a one-electron slope at short times (<1 s). The Figure 6B behavior is that predicted[20] for an ECE process with a slow intermediate chemical step or steps, according to[20a]

$$i = FAC_{ox}\left(\frac{D}{\pi t}\right)^{1/2}\{n + n'(1 - \exp[-kt])\} \qquad (2)$$

In the limit of $k = 0$, and $n = n' = 1$, this equation reduces to the Cottrell equation and, for very large k, to twice the Cottrell equation. Application to Figure 6B as a plot of $\ln\{2 - i(\pi t)^{1/2}/FACD^{1/2}\}$ vs. t (Figure 6D) shows that the data give a good correlation with the equation. The slope of the plot gives $k = 0.5$ s^{-1}, which is the overall rate constant under the specific conditions of the experiment. We emphasize that this rate constant is potentially a *composite* of the on–off rates of all axial ligands and of dioxygen binding in Scheme I. Axial bases are known to be important to the reactivity of high-valent oxo–porphyrins[9] in similar systems involving oxygen activation. In Scheme I, the axial base represents a potentially rate limiting step in the *generation* of the high-valent complex. In principle, Scheme I could be dissected to locate the RDS, but we have not attempted the

(16) Dolphin, D.; James, B. *ACS Symp. Ser.* **1983**, *No. 211*, 99.
(17) (a) Sligar, S.; Kennedy, K.; Pearson, D. *Proc. Natl. Acad. Sci. U.S.A.* **1980**, *77*, 1240. (b) White, R. E.; Coan, M. J. *Annu. Rev. Biochem.* **1980**, *49*, 315.
(18) (a) Khenkin, A. M.; Shteinman, A. A. *Oxid. Commun.* **1983**, *4*, 433. (b) Khenkin, A. M.; Shteinman, A. A. *J. Chem. Soc., Chem. Commun.* **1984**, 1219.
(19) (a) Bartolini, O.; Meunier, B. *J. Chem. Soc., Chem. Commun.* **1983**, 1364. (b) Carnier, N.; Harriman, A.; Porter, G. *J. Chem. Soc., Dalton Trans.* **1982**, 931.
(20) (a) Murray, R. W. In *Physical Methods of Chemistry*; Rossiter, B. W., Hamilton, J. F., Eds.; Wiley-Interscience: New York, 1986; Vol. 2, p 547. (b) This equation assumes an irreversible chemical reaction in the ECE sequence, but the more complex expression for a reversible chemical step reduces to nearly the same form. See: Alberts, G. S.; Shain, I. *Anal. Chem.* **1963**, *35*, 1859.

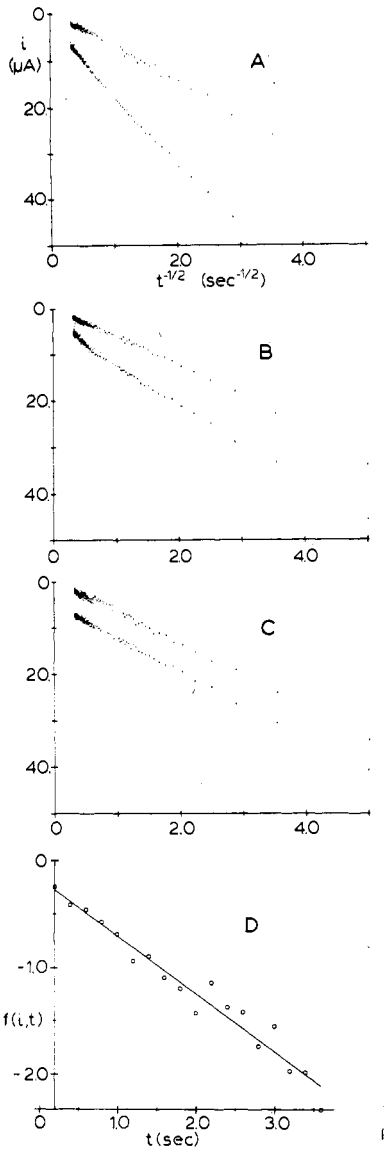

Figure 6. Chronoamperometry (Cottrell plots) of Mn(TPP)Bzo (1.0 mM), in dichloromethane–0.5 M Bu_4NClO_4, with and without oxygen: (A) nothing added; (B) solution in (A) with 1-methylimidazole (3 mM); (C) solution in (A) with 1-methylimidazole (3 mM) and benzoic anhydride (0.1 M); (D) kinetic plot of eq 1 to determine ECE rate constant (see text).

necessary detailed kinetic analysis.

The effect of added anhydride on the chronoamperometric response is shown in Figure 6C. Analogous to the rotated-disk voltammetry in Figure 4A (▲) with anhydride and oxygen present, the Cottrell plot exhibits a non-zero current intercept, again evidence for the catalytic regeneration current caused by the reactions of Scheme II.

Controlled-Potential Electrolysis. The rotated-disk and chronoamperometric results for the acid anhydride reaction step show that its rate corresponds to the slowest time scale accessible in these experiments. The longer experimental time scales (hours) of controlled-potential electrolysis in stirred solution allows the acid anhydride reaction to display larger electrochemical effects, as displayed in Figure 7.

Electrolysis of a solution of Mn(TPP)Bzo in the absence of dioxygen (Figure 7, curves A) gives current and charge–time curves that level off as reduction to the Mn(II) complex is completed. The charge passed (0.366 C) agrees with that expected for one electron (0.390 C, ---). When the solution is oxygenated (Figure 7, curves B), the currents and charges are larger, and the charge is approximately that expected for the two-electron process of Scheme I. The current in curve B does not fall to zero as in curve A; on this long time scale some further current appears to

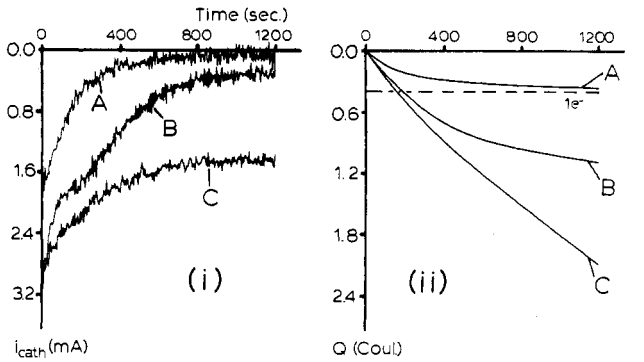

Figure 7. Controlled-potential electrolysis (−0.5 V) of Mn(TPP)Bzo (3.2 mg = 4.05 μmol) with 1-methylimidazole (5 mM) present: (A) with no anhydride, under argon; (B) with no anhydride, under dioxygen; (C) with benzoic anhydride (0.1 M), under dioxygen. Charge vs. time data (panel ii) were obtained by digital integration of the current (panel i).

be passed probably by reaction of the $Mn^{III}(TPP)O_2^{2-}$ complex with trace protonic impurities, regenerating $Mn^{III}(TPP)Bzo$.

With both dioxygen and benzoic anhydride present, on the other hand, the current (Figure 7, curve C) reaches a much larger, steady value (ca. 1.5 mA) so that the corresponding charge passed grows linearly with time. The steady-state current is very persistent, and continuation of the electrolysis for 1 h (not shown) resulted in passage of a charge corresponding to 16 reductive turnovers of the Mn(TPP)Bzo complex. These results clearly support a catalytic reduction of dioxygen via Scheme II.

The slope of the charge–time curve of Figure 7ii, curve C, reflects the kinetics[21] of the catalytic regeneration in Scheme II. This is a key step in maximizing epoxidation efficiency by using electrochemically generated high-valent porphyrins, and further studies of this issue are ongoing.

Experimental Section

Reagents. Dichloromethane was purified by washing with concentrated sulfuric acid, water, and 0.5 M sodium bicarbonate, drying over anhydrous sodium sulfate, and distilling from calcium hydride and was stored in brown bottles over 4A molecular sieves. Supporting electrolyte (n-Bu_4NClO_4), prepared from tetrabutylammonium bromide and perchloric acid, was recrystallized three times from ethyl acetate. Benzoic anhydride was washed with aqueous bicarbonate and water to remove acid impurities and crystallized from benzene–hexane. Tetramethylammonium benzoate was prepared by the method of Volz and Ruchti[22] and the water removed by azeotropic distillation in toluene. The product was dried at room temperature under vacuum (10^{-2} Torr). Other chemicals were reagent grade and were used as received.

Mn(TPP)Cl. Free base H_2TPP, the generous gift of Dr. Scott Raybuck, was synthesized by the condensation of pyrrole and benzaldehyde and was freed of chlorin impurity by reaction with dichlorodicyanobenzoquinone.[3] Manganese was inserted into the macrocycle by the standard method[3] of reflux with excess $MnCl_2$ (Aldrich) in DMF. The product was dissolved in benzene and treated with aqueous NaCl to assure complete metathesis to the chloride complex. Finally, the Mn(TPP)Cl product was purified by recrystallization from benzene–heptane. The final product was found to be pure by TLC (silica gel, CH_2Cl_2) and visible spectroscopy.

Exchange of the Coordinated Anion. To exchange the chloride anion for bromide, acetate, or benzoate, the following general procedure was followed. A quantity (approximately 25 mg) of Mn(TPP)Cl dissolved in 50 mL of dichloromethane was treated in a separatory funnel with a dilute aqueous solution of the sodium salt of the desired anion. This procedure was repeated, followed by a final wash with distilled water. The organic layer is collected, dried over anhydrous sodium sulfate, and reduced to 5 mL under reduced pressure. Crystallization of the product was induced by slow addition of heptane. Purity was confirmed by visible spectroscopy and cyclic voltammetric behavior.

Mn(p-MeOTPP)X. Free base H_2-p-MeOTPP was purchased from Aldrich and used as received. Manganese was inserted by a procedure similar to that described above, except that $Mn(OAc)_2$ was used instead of $MnCl_2$. The final product of the insertion procedure was the acetate

(21) Bard, A. J.; Santhanam, K. S. V. In *Electroanalytical Chemistry*; Bard, A. J., Ed.; Marcel Dekker: New York, 1971; Vol. 4.
(22) Volz, H.; Ruchti, L. *Liebigs Ann. Chem.* **1977**, 33.

complex, from which the benzoate and chloride complexes were prepared by the above metathesis procedure.

Mn(TMP)Bzo. Mn(TMP)Cl was the generous gift of Dr. Scott Raybuck and was used in the above metathesis procedure to prepare the benzoate complex.

Electrochemical Instrumentation. Cyclic voltammetry was performed with a potentiostat and waveform generator of local construction. Rotated-disk voltammetry was performed with the same potentiostatic hardware and a Pine Instruments Model ASR-2 variable-speed analytical rotator. Chronoamperometry and controlled-potential electrolysis experiments were performed with a PAR 173 potentiostat and PAR 176 current-to-voltage converter. Potential steps were generated and current–time data recorded with the aid of an IBM-PC computer with a Tecmar Labmaster 12-bit analog-to-digital converter. In chronoamperometry experiments, background currents were recorded on blank solutions and subtracted digitally.

Electrochemical Experiments. All experiments were performed in dichloromethane–0.2 M n-Bu_4NClO_4. Glassy-carbon-disk working electrodes (Atomergic, grade V-10, 0.057 cm^2) were pressure-fitted into Teflon, polished with 1-μm diamond paste (Buehler) on a manila surface and rinsed with copious quantities of water and dichloromethane. Potentials are reported vs. the NaCl saturated calomel electrode (NaSCE). Solutions were purged with argon and oxygenated with pure oxygen.

Cyclic voltammetry and rotated-disk voltammetry were performed in a conventional two-component cell with the working electrode and platinum-wire counter electrode in the same compartment. Chronoamperometry was performed in a similar cell, except that a Luggin capillary connected the cell compartments, to diminish the effects of uncompensated solution resistance. Controlled-potential electrolysis experiments were performed with a glassy-carbon crucible (Atomergic, grade V-25) as both working electrode and reaction vessel.

Acknowledgment. Helpful discussions with Prof. J. P. Collman and J. Fitzgerald of Stanford University and Dr. Scott Raybuck of the Massachusetts Institute of Technology are gratefully acknowledged. This work was supported in part by a grant from the National Science Foundation. S.E.C. acknowledges support from the 1986 Edward G. Weston Fellowship of The Electrochemical Society.

Contribution from the Departments of Chemistry, University of Denver, Denver, Colorado 80208, and University of Colorado at Denver, Denver, Colorado 80202

Metal–Nitroxyl Interactions. 52. EPR Spectra of Nitroxyl Radicals Coordinated to Manganese(III) Tetraphenylporphyrin via the Nitroxyl Oxygen

Kundalika M. More, Gareth R. Eaton,* and Sandra S. Eaton*

Received February 24, 1987

EPR spectra of six nitroxyl radicals coordinated to manganese(III) tetraphenylporphyrin via the nitroxyl oxygen were examined in frozen toluene solution. Antiferromagnetic coupling between the $S = 2$ Mn(III) and the $S = {}^1/_2$ nitroxyl states resulted in an $S = {}^3/_2$ ground state. The observed effective g values of 4.0 and 2.0 are characteristic of zero-field splitting greater than the EPR quantum. Resolved nuclear hyperfine splitting was observed on the $g = 4$ signal. The antiferromagnetic interaction was sufficiently strong that the $S = {}^5/_2$ excited state was not detected at 100 K.

Introduction

Electron–electron spin–spin interaction between nitroxyl radicals and paramagnetic transition metals has been observed in two classes of compounds.[1] (1) The nitroxyl is part of a ligand that is bound to the metal by an atom other than the nitroxyl oxygen. (2) The nitroxyl oxygen is coordinated to the metal. For complexes of the first type, a range of magnitudes of spin–spin interaction has been analyzed by EPR.[1] For the second type of complex, relatively little EPR data have been obtained for the following reasons. Many of the studies of coordination of nitroxyl radicals to transition metals have used metals with $S = {}^1/_2$, particularly Cu(II). Spin–spin interaction between two $S = {}^1/_2$ centers results in a singlet (which does not give an EPR spectrum) and a triplet. When the nitroxyl oxygen is bound to the $S = {}^1/_2$ metal the M–O distance is about 2.0 to 2.5 Å.[2] As a result of the short interspin distance there is large dipolar interaction that can make detection of the triplet EPR signal difficult. In addition, in many of the cases that have been examined the spin–spin interaction is strongly antiferromagnetic and the population of the triplet is small. As a result no EPR spectra have been reported for complexes in which a nitroxyl oxygen is bound to a metal with $S = {}^1/_2$ and the coupling is antiferromagnetic. Triplet EPR spectra have been obtained for a complex with a nitroxyl oxygen bound to Cu(II) in which the coupling was ferromagnetic.[3] If the metal has $S > {}^1/_2$, spin coupling to one or more bound nitroxyl radicals can produce species with an odd number of unpaired electrons. EPR spectra should then be readily detectable for the lowest Kramer's doublets in these systems. Room-temperature EPR spectra in magnetically concentrated solids were recently reported for the $S = {}^3/_2$, ${}^5/_2$, and ${}^7/_2$ spin states that result from antiferromagnetic coupling between Mn(II) and two nitroxyl radicals.[4] In this paper we report that an $S = {}^3/_2$ spin state results when nitroxyl radicals I–VI are coordinated to Mn(III) tetraphenylporphyrin ($S = 2$) in dilute solution.

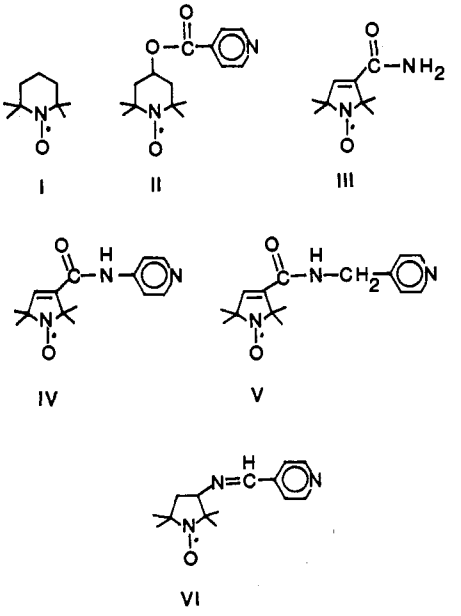

* To whom correspondence should be addressed: G.R.E., University of Denver; S.S.E., University of Colorado at Denver.

(1) Eaton, S. S.; Eaton, G. R. *Coord. Chem. Rev.*, in press.
(2) Felthouse, T. R.; Dong, T.-Y.; Hendrickson, D. N.; Shieh, H.-Y.; Thompson, M. R. *J. Am. Chem. Soc.* **1986**, *108*, 8201.
(3) Bencini, A.; Benelli, C.; Gatteschi, D.; Zanchini, C. *J. Am. Chem. Soc.* **1984**, *106*, 5813.
(4) Benelli, C.; Gatteschi, D.; Zanchini, C.; Doedens, R. J.; Dickman, M. H.; Porter, L. C. *Inorg. Chem.* **1986**, *25*, 3453.

0020-1669/87/1326-2618$01.50/0